Orbital Evolution of Extreme-Mass-Ratio Black-Hole Binaries with Numerical Relativity

Carlos O. Lousto and Yosef Zlochower

Center for Computational Relativity and Gravitation and School of Mathematical Sciences, Rochester Institute of Technology, 85 Lomb Memorial Drive, Rochester, New York 14623, USA

(Received 1 September 2010; published 24 January 2011)

We perform the first fully nonlinear numerical simulations of black-hole binaries with mass ratios 100:1. Our technique is based on the moving puncture formalism with a new gauge condition and an optimal choice of the mesh refinement. The evolutions start with a small nonspinning black hole just outside the ISCO that orbits twice before plunging. We compute the gravitational radiation, as well as the final remnant parameters, and find close agreement with perturbative estimates. We briefly discuss the relevance of these simulations for Advanced LIGO, third-generation ground-based detectors, LISA observations, and self-force computations.

DOI: 10.1103/PhysRevLett.106.041101 PACS numbers: 04.25.dg, 04.25.Nx, 04.30.Db, 04.70.Bw

Introduction.—The orbital evolution and computation of gravitational radiation from black-hole binaries (BHB) in the small-mass-ratio limit remains one of the most challenging problems in general relativity. This was recognized early on by Regge and Wheeler over 50 years ago [1]. Zerilli then completed the formulation of the first order perturbations around a Schwarzschild BH in 1970 [2]. Three years later, Teukolsky [3] provided a new formalism to study perturbations around Kerr BHs. In order to take into account the decay of the orbit of the small BH due to the emission of gravitational radiation, second order effects have to be included in those computations. This problem turned out to be very challenging, and only since 1996 [4,5] has there been a consistent formalism for the "self-force" corrections to the background geodesic motion of a small BH orbiting around a larger one. The explicit implementation of such formalism into a computational scheme remains challenging, although recent progress along this line is encouraging [6].

The dramatic breakthroughs in the numerical techniques to evolve BHBs [7–9] transformed the field of numerical relativity (NR) and we are now in a position to evolve binary systems in the intermediate mass ratio regime. Two years ago the merger of spinning [10] binaries with mass ratio $q = m_1/m_2 = 1/8$ and nonspinning binaries [11] with $q = 1/10$ were published. More recently, detailed long term evolutions of BHBs with $q = 1/10$ and $q = 1/15$ were studied and validated against perturbation theory [12,13]. In this Letter we present the first fully nonlinear numerical simulations of the merger of small-mass-ratio BHBs. As a case study, we evolve an initially nonspinning BHB with mass ratio $q = 1/100$ for over two orbits prior to merger, and resolve the entire waveform for three grid resolutions, proving numerical convergence of the results. The success of our approach is based on enhancements of the moving puncture numerical techniques that adapt the gauge and grid structure to the small-mass-ratio limit.

The techniques described in this Letter can be used in the spinning BHB case and for even smaller mass ratio inspirals. This has important consequences for astrophysics and gravitational wave observatories such as the second-generation advanced LIGO detector, third-generation ground-based detectors, and LISA. Supermassive BH collision at cosmological scales are most likely to occur in the mass ratio range $1{:}10 - 1{:}100$ [14] and will be observable by LISA, while collision of intermediate mass BHs and solar mass BHs will lie in the sensitivity band of second and third generation ground-based detectors [15–17].

Fully nonlinear numerical simulations.—In Table I we give the initial data parameters for our $q = 1/100$ BHB simulations. We evolved this BHB data set using the LAZEV [18] implementation of the moving puncture approach [8,9]. Our code used the CACTUS-EINSTEIN toolkit [19,20] and the CARPET [21] mesh refinement driver to provide a "moving boxes" style mesh refinement. We use AHFINDERDIRECT [22] to locate apparent horizons. We measure the magnitude of the horizon spin using the isolated horizon algorithm detailed in [23].

We obtain accurate, convergent waveforms and horizon parameters by evolving this system in conjunction with a modified 1 + log lapse and a modified Gamma-driver shift condition [8,24], and an initial lapse $\alpha(t = 0) = 2/(1 + \psi_{\rm BL}^4)$. The lapse and shift are evolved with $(\partial_t - \beta^i \partial_i)\alpha = -2\alpha K$, $\partial_t \beta^a = \frac{3}{4}\tilde{\Gamma}^a - \eta(x^k, t)\beta^a$, where different functional dependences for $\eta(x^k, t)$ have been proposed

TABLE I. Initial data parameters. The punctures are located on the x axis at positions x_1 and x_2, with puncture mass parameters m_1 and m_2, and momentum $\pm\vec{p}$. The punctures have zero spin. The ADM mass $M_{\rm ADM}$ is $1M$ and $q = 0.010\,000\,04$.

x_1	4.952 56	x_2	−0.047 437 4	p_x	−0.000 010 265 2
p_y	0.006 722 62	m_1	0.008 689 47	m_2	0.989 619

in [18,25–29]. Here we use a modification of the form proposed in [26], $\eta(x^k, t) = R_0\sqrt{\tilde{\gamma}^{ij}\partial_i W \partial_j W}/((1 - W^a)^b)$, where we chose $R_0 = 1.31$ and W is the evolved conformal factor. The above gauge condition is inspired by, but differs from, Ref. [26] between the BHs and in the outer zones when $a \neq 1$ and $b \neq 2$. Once the conformal factor settles down to its asymptotic $\psi = C/\sqrt{r} + O(1)$ form near the puncture, η will have the form $\eta = (R_0/C^2)(1 + b(r/C^2)^a)$ near the puncture and $\eta = R_0 r^{b-2} M/(aM)^b$ as $r \to \infty$. Our exploration of the (a, b) parameters showed that the (1, 2) case leads to numerical instabilities on coarse grids, while the (2, 1) and (1, 1) cases lead to noisy waveforms and slower gauge speeds. In practice we used $a = 2$ and $b = 2$, which reduces η by a factor of 4 at infinity when compared to the original version of this gauge proposed by [26]. We note that if we set $b = 1$ then η will have a $1/r$ falloff at $r = \infty$ as suggested by [28].

In order to chose the width of the refinement levels closest to the small BH, we examine the potentials for perturbations about a nonspinning BH. The idea is that we need to model the curvature and the gravitational radiation emitted by the small BH (which drives the merger, and hence the physics). At the zeros of the derivative of the potentials, the variations are minimized. Furthermore the separations between zeros increases, naturally leading to a choice of small-width, high resolution grids between the first zeros, one step lower in resolution between the second two, followed by a sequence of coarser grids. According to Chandrasekhar ([30], p. 160) the even-odd ($\pm$) parity effective potentials of a Schwarzschild BH can be written as

$$V_\ell^\pm = \pm 6M\frac{df}{dr^*} + (6M)^2 f^2 + 4\lambda(\lambda + 1)f, \qquad (1)$$

where

$$f = \frac{(r - 2M)}{2r^2(\lambda r + 3M)}, \qquad \lambda = \frac{1}{2}(\ell + 2)(\ell - 1). \qquad (2)$$

Note that both potentials are numerically very close to each other, hence we consider the vanishing of the derivative of the average of the two (in isotropic coordinates R) when constructing the grid. For $\ell = 2$ and $M = 1$ this takes the explicit form

$$\left.\frac{d(V^+ + V^-)}{dR}\right|_{\ell=2,M=1} = -384\frac{R(2R - 1)(16R^4 - 4R^3 - 60R^2 - R + 1)}{(2R + 1)^9(4R^2 + 10R + 1)^3} \times (64R^6 + 288R^5 + 480R^4 + 256R^3 + 120R^2 + 18R + 1). \qquad (3)$$

Ideally, we would like to place the AMR boundaries around the small BH near the zeros of this function ($R/m = 0.0$, $0.120\,799\,843\,1$, 0.5, $2.069\,539\,112$) The location of the zeros for $\ell > 2$ changes little from the above figures. Since we do not want to over-resolve the interior, this suggests that the first grid level should cover the whole small hole up to its horizon, and the next grid level up to 4 times the initial horizon radius of the small hole in the initial quasi-isotropic coordinates.

In Ref. [13] we provide an alternative method of extrapolation of waveforms based on a perturbative propagation of the asymptotic form of ψ_4 at large distances, leading to the following simple expression

$$\lim_{r\to\infty}[r\psi_4^{\ell m}(r, t)] = [r\psi_4^{\ell m}(r, t) - \lambda\int_0^t dt\,\psi_4^{\ell m}(r, t)]_{r=r_{\rm Obs}} + O(r_{\rm Obs}^{-2}), \qquad (4)$$

where $r_{\rm Obs}$ is the approximate areal radius of the sphere. This formula is applicable for $r_{\rm Obs} \gtrsim 100M$. And note that it is also important to remove the low frequency components [31] in ψ_4 (since it is inside an integral).

Results and Analysis.—Our simulation used 15 levels of refinement (around the smaller components), with central resolutions as high as $M/7078$, and 9 levels of refinement around the larger component. The outer boundaries were located at $400M$ and the resolution in the boundary zone was $h = 2.3148M$ for our finest resolution run. The BHB performs $\sim$2 orbits prior to merger [as seen by the formation of a common apparent horizon (CAH)], which occurs roughly $150M$ after the start of the simulation. In terms of computational expense, a medium resolution run requires 500 000 SU and approximately one month of runtime. In order to reduce the total runtime, we used an aggressive choice of the CFL (Courant-Friedrichs-Lewy) factor ($dt = 1/2h$), which leads to significant BH mass loss when compared to $dt = 1/4h$.

Table II shows the results of evolution. We note that the smaller BH mass is conserved to within 0.23% during the inspiral and plunge phases, while the mass of the larger BH is conserved to within 0.003%. In Fig. 1 we show the xy projections of the orbital trajectories. From the figure we can see that the initial jump in the orbit pushes the binary slightly outside the ISCO, leading to an additional orbit. In Fig. 2 we show the orbital radius as a function of time and resolution. Note that the orbital radius superconverges at low resolution and converges quadratically at high resolution (this quadratic error may be due to time prolongation

TABLE II. Remnant horizon parameters and radiated energy momentum. Here we provide $\delta M_H^* = M_{\rm ADM} - M_H$ and $\delta S_H^* = J_{\rm ADM} - S_H$, which are small numbers obtained by taking the difference between two much larger numbers. The calculation of δS_H^* is relatively inaccurate because it requires an extrapolation to infinite resolution.

$10^5 E_{\rm rad}$	6.0 ± 0.1	$10^5\delta M_H^*$	7.0 ± 1.0	100α	3.33 ± 0.02
$10^4 J_{\rm rad}$	5.0 ± 0.2	$10^4\delta S_H^*$	3.0 ± 2.0	$V_{\rm kick}$	1.07 ± 0.05 km/s

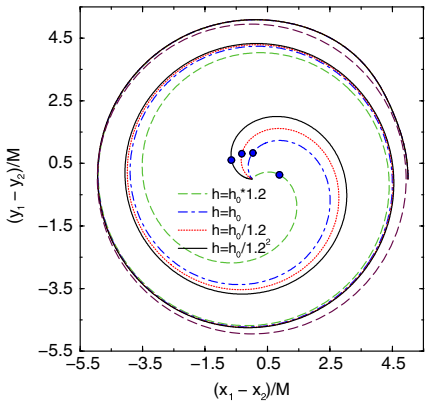

FIG. 1 (color online). An xy projection of the trajectories for the two highest resolutions of the $q = 1/100$ configuration. The dotted circle corresponds to the ISCO radius while the small filled-in circle corresponds to the point on the trajectory where a common horizon is first detected. Note the initial "jump" in radius (see Fig. 2) due to the initial data radiation content.

effects, as well as effects due to an aggressive choice of the CFL factor). In Fig. 3 we show amplitude, as well as phase convergence, of the $(\ell = 2, m = 2)$ mode of ψ_4.

The apparent superconvergence in the trajectories and waveforms when considering the three coarsest resolutions is indicative that the lowest resolution is just entering the convergence regime. That is, this resolution cannot be far from the convergence regime because all four resolutions lie in a monotonic convergence sequence. And importantly, the deviations between the next three resolutions are very small compared to the deviation between the lowest two resolutions, indicating that these three resolutions are safely inside the convergence regime.

Finally, in Fig. 4 and Table III we show the remnant spins and total radiated mass as a function of mass ratio [13] for $q = 1/10, 1/15, 1/100$ and the predictions based

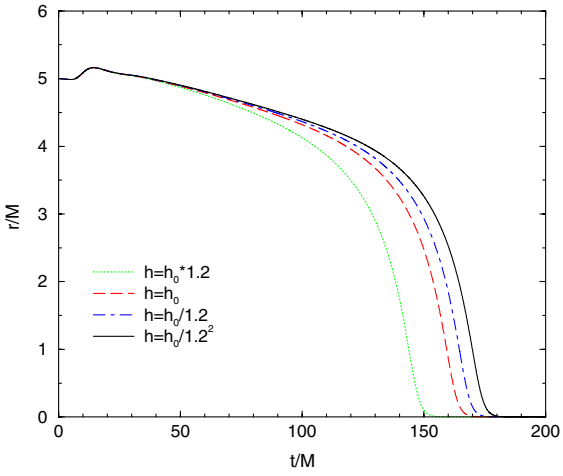

FIG. 2 (color online). The orbital radius as a function of time and resolution for the $q = 1/100$ configuration. Note the initial "jump" in the orbit due to the initial data.

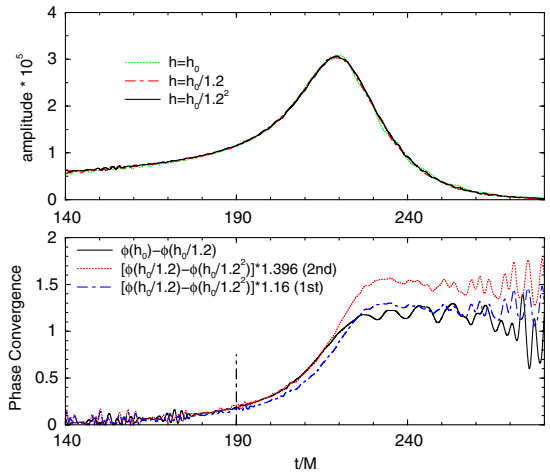

FIG. 3 (color online). Convergence of the amplitude and phase of the $(\ell = 2, m = 2)$ mode of ψ_4. The phase converges to second order prior to the peak in the amplitude. The vertical line shows the point when $\omega = 0.2$. Note the good agreement in amplitude (the curves have been translated). The phase error at $\omega = 0.2$ is 0.44 radians. The reduced order of convergence is due to an aggressive choice of the CFL factor.

on our empirical formula [32]. Note that no fitting is involved in this figure.

The amount of energy and angular momentum radiated when the (2,2) mode frequency is larger than $M\omega_{2,2} > 0.167$ is given by (adding up to $\ell = 4$ modes) $\delta E/M = 0.000\,047 \pm 0.000\,001$ and $\delta J/M^2 = 0.000\,34 \pm 0.000\,01$, which agrees to within 4% with the particle limit predictions of $\delta E/M = 0.47\eta^2$ and $\delta J/M^2 = 3.44\eta^2$ of Ref. [33].

Conclusions and Discussion.—We have successfully evolved a 1:100 BHB system for the last two orbits before merger and down to the final Kerr hole remnant. We have achieved this within the moving punctures approach by adapting the gamma-driver shift condition with a variable

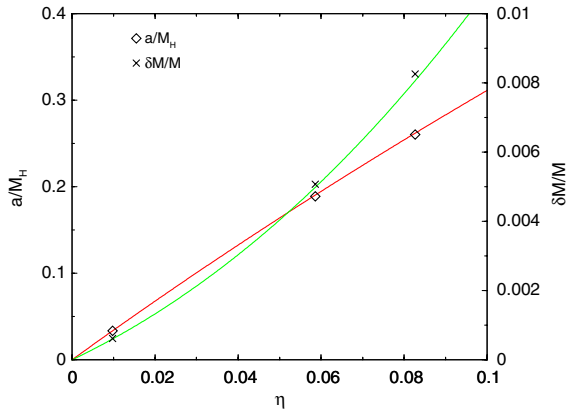

FIG. 4 (color online). The remnant spin a/M_H and the radiated mass from infinite separation $\delta M/M$, as a function of the symmetric mass ratio $\eta = q/(1+q)^2$, for $q = 1/10$, $1/15$, $1/100$, as well as the empirical formula prediction.

TABLE III. Remnant spin and total radiated mass (starting from infinite separation) as a function of mass ratio q as measured in our simulations and as predicted by our empirical formulas [32].

q	1/10	1/15	1/100
α (computed)	0.2603	0.188 75	0.0333
α (predicted)	0.2618	0.1903	0.033 58
δM (computed)	0.008 26	0.005 07	0.000 618
δM (predicted)	0.008 06	0.004 98	0.000 604

damping term. Also crucial for evolutions is an optimal choice of the mesh refinement structure around the small BH. We used the Regge-Wheeler-Zerilli potentials to guide the setting up of the initial grids. This helps optimizing the large resources required to evolve small q binaries. The numerical convergence of the waveforms displayed here, and the successful comparisons with perturbative results [12,13], show this approach is validated in the intermediate mass ratio regime, and can be applied to even smaller q's (and larger initial separations into the post-Newtonian regime).

The feasibility of simulating extreme mass ratios by purely fully nonlinear numerical methods, as demonstrated in this work, allows us to look more optimistically at the task of generating a bank of templates for second and third generation ground-based detectors and LISA. Methods like those described in [12,13], that combine NR and perturbative techniques can be used to speed up the generation of those templates. And finally we now also have a direct way of validating self-force computations [6].

The techniques presented here would appear to apply in a straightforward manner to even smaller mass ratios q and to initially spinning BHs. Fine tuning of the quasicircular orbital parameters plays an important role in preparing these runs, given the very low level of gravitational radiation they generate. So far we see that the method [34] developed for equal mass BHBs to lower the eccentricity works, but it requires extra runs for initial experimentation. Hence it would be important to evolve initial data with lower spurious radiation content and some true inspiral wave information [35].

We gratefully acknowledge the NSF for financial support from Grants No. PHY-0722315, No. PHY-0653303, No. PHY-0714388, No. PHY-0722703, No. DMS-0820923, No. PHY-0929114, No. PHY-0969855, No. PHY-0903782, No. CDI-1028087; and NASA for financial support from NASA Grants No. 07-ATFP07-0158 and No. HST-AR-11763. Computational resources were provided by the Ranger cluster at TACC (Teragrid allocation TG-PHY060027N) and by NewHorizons at RIT.

[1] T. Regge and J. Wheeler, Phys. Rev. **108**, 1063 (1957).
[2] F. J. Zerilli, Phys. Rev. D **2**, 2141 (1970).
[3] S. A. Teukolsky, Astrophys. J. **185**, 635 (1973).
[4] Y. Mino, M. Sasaki, and T. Tanaka, Phys. Rev. D **55**, 3457 (1997).
[5] T. C. Quinn and R. M. Wald, Phys. Rev. D **56**, 3381 (1997).
[6] L. Barack and N. Sago, Phys. Rev. D **81**, 084021 (2010).
[7] F. Pretorius, Phys. Rev. Lett. **95**, 121101 (2005).
[8] M. Campanelli, C. O. Lousto, P. Marronetti, and Y. Zlochower, Phys. Rev. Lett. **96**, 111101 (2006).
[9] J. G. Baker, J. Centrella, D.-I. Choi, M. Koppitz, and J. van Meter, Phys. Rev. Lett. **96**, 111102 (2006).
[10] C. O. Lousto and Y. Zlochower, Phys. Rev. D **79**, 064018 (2009).
[11] J. A. Gonzalez, U. Sperhake, and B. Brugmann, Phys. Rev. D **79**, 124006 (2009).
[12] C. O. Lousto, H. Nakano, Y. Zlochower, and M. Campanelli, Phys. Rev. Lett. **104**, 211101 (2010).
[13] C. O. Lousto, H. Nakano, Y. Zlochower, and M. Campanelli, Phys. Rev. D **82**, 104057 (2010).
[14] M. Volonteri and P. Madau, Astrophys. J. **687**, L57 (2008).
[15] I. Mandel, D. A. Brown, J. R. Gair, and M. C. Miller, Astrophys. J. **681**, 1431 (2008).
[16] I. Mandel and J. R. Gair, Classical Quantum Gravity **26**, 094036 (2009).
[17] C. M. Will, Astrophys. J. **611**, 1080 (2004).
[18] Y. Zlochower, J. G. Baker, M. Campanelli, and C. O. Lousto, Phys. Rev. D **72**, 024021 (2005).
[19] CACTUS: http://www.cactuscode.org/
[20] EINSTEIN Toolkit home page: http://einsteintoolkit.org.
[21] E. Schnetter, S. H. Hawley, and I. Hawke, Classical Quantum Gravity **21**, 1465 (2004).
[22] J. Thornburg, Classical Quantum Gravity **21**, 743 (2004).
[23] O. Dreyer, B. Krishnan, D. Shoemaker, and E. Schnetter, Phys. Rev. D **67**, 024018 (2003).
[24] M. Alcubierre, B. Brügmann, P. Diener, M. Koppitz, D. Pollney, E. Seidel, and R. Takahashi, Phys. Rev. D **67**, 084023 (2003).
[25] M. Alcubierre *et al.*, arXiv:gr-qc/0411137.
[26] D. Mueller and B. Bruegmann, Classical Quantum Gravity **27**, 114008 (2010).
[27] D. Müller, J. Grigsby, and B. Brügmann, Phys. Rev. D **82**, 064004 (2010).
[28] E. Schnetter, Classical Quantum Gravity **27**, 167001 (2010).
[29] D. Alic, L. Rezzolla, I. Hinder, and P. Mosta, Classical Quantum Gravity **27**, 245023 (2010).
[30] S. Chandrasekhar, *The Mathematical Theory of Black Holes* (Oxford University Press, Oxford, U.K., 1983).
[31] C. Reisswig and D. Pollney, arXiv:1006.1632.
[32] C. O. Lousto, M. Campanelli, Y. Zlochower, and H. Nakano, Classical Quantum Gravity **27**, 114006 (2010).
[33] S. Bernuzzi and A. Nagar, Phys. Rev. D **81**, 084056 (2010).
[34] H. P. Pfeiffer *et al.*, Classical Quantum Gravity **24**, S59 (2007).
[35] B. J. Kelly, W. Tichy, Y. Zlochower, M. Campanelli, and B. F. Whiting, Classical Quantum Gravity **27**, 114005 (2010).